J Mater Sci (2013) 48:1819–1825
DOI 10.1007/s10853-012-6946-5

Metallic glass formation in the binary Cu–Hf system

I. A. Figueroa · J. D. Plummer · G. A. Lara-Rodriguez · O. Novelo-Peralta · I. Todd

Received: 3 August 2012 / Accepted: 9 October 2012 / Published online: 20 October 2012

Abstract Glass formation, structure and thermal properties of alloys in the binary $Cu_{100-x}Hf_x$ alloy system, where $x = 25$–50 at.%, are reported and discussed. This work also presents a comparison between copper casting techniques, from thick melt-spun ribbons to suction cast cylindrical rods, and the prediction of critical diameter, d_c, based on maximum ribbon thickness, x_c. Ribbons of $Cu_{60}Hf_{40}$ and $Cu_{65}Hf_{35}$ exhibited a fully glassy phase up to a thickness of 170 μm. Suction casting lead to an increase in the largest diameter over which both alloys could be cast, in comparison to melt-spun ribbons, and remain amorphous, with $Cu_{65}Hf_{35}$ showing a large critical diameter of 1 mm. This result is rationalised by a lower liquidus temperature, T_l, which maximises the reduced glass transition temperature, T_{rg}, and also correlates closely with the eutectic point. Finally, there were remarkable similarities between the Miedema model and the efficient packing model for predicting the range for metallic glass formation in this binary system.

I. A. Figueroa (✉) · G. A. Lara-Rodriguez · O. Novelo-Peralta
Instituto de Investigaciones en Materiales, Universidad Nacional Autónoma de México, 04510 Mexico, DF, Mexico
e-mail: iafigueroa@iim.unam.mx

J. D. Plummer
Department of Materials, Royal School of Mines, Imperial College London, Prince Consort Road, London SW7 2BP, UK

J. D. Plummer · I. Todd
Department of Materials Science and Engineering, University of Sheffield, Sir Robert Hadfield Building, Mappin Street, Sheffield, South Yorkshire S1 3JD, UK

Introduction

Binary alloys have generally been recognised as exhibiting only poor or, at best, moderate glass formability; being composed of only two constituent elements, the potential for dense random packing of atoms is lower than can be achieved for multicomponent alloys with favourable ratios of atomic diameters. Additionally, the degree of atomic rearrangement required for crystallisation is smaller than that for the ternary or higher order alloys. Binary alloys thus generally require higher cooling rates to suppress crystallisation than multicomponent alloys. The resultant binary metallic glasses have a more restricted specimen geometry, such as thin ribbons, foils and powders. However, Guo et al. [1] reported bulk glass formation (defined as exhibiting a fully amorphous structure over a limiting dimension of at least 1 mm) in the binary $Ca_{66.4}Al_{33.6}$ alloy, which was the first bulk metallic glass (BMG) produced in a bi-metallic system using the copper mould injection casting method. Subsequently, Tang et al., Duan et al. and Inoue et al. [2–4] reported fully amorphous 2 mm thick strips of $Cu_{64}Zr_{36}$ and $Cu_{66}Hf_{34}$. With the discovery of these binary BMGs, the scientific community showed more interest in this research area.

Xia et al. [5] reported the glass-forming ability (GFA) of Cu–Hf and Cu-rich binary alloys, finding 2 mm diameter BMG rods using conventional Cu-mould casting. Alloys with the highest γ^* parameter ($T_x/[T_l - T_g]$), which is one of the most recent thermodynamic descriptors for evaluating GFA, were found beyond the $Cu_{61.4}Hf_{38.6}$ eutectic. Jia et al. [6] reported optimised compositions for BMGs in the Cu–Hf system, where the fragility parameter, D^*, of $Cu_{55}Hf_{45}$ was calculated. The concept of fragility, proposed by Angell [7], is a classification scheme describing the temperature dependence of viscosity. It is believed that

D^* is on the order of 2 for the most fragile liquids and 100 for the strongest glass formers, such as SiO_2 [8].

This type of bulk vitreous material has recently been the subject of theoretical studies on the fundamentals of glass formation [9], because of the simplicity of binary alloys and the advantage this offers in high value experimental studies such as high energy X-ray and neutron diffraction. Basu et al. [9] reported an approach using Miedema's model [10] for determining the glass-forming composition range for a particular alloy system. They theoretically determined the glass-forming composition range for different binary and ternary (Zr, Ti, Hf)–(Cu, Ni) alloys. It was concluded that in the Cu–Hf system glass-forming compositions could be approximately found in the range 10–80 at.% Hf. In addition, Li et al. [11] presented some theoretical calculations which suggested that the optimum glass-forming composition range fell between $x_{Hf} = 32$ and 38 at.% in the Cu–Hf system. This result was based on thermodynamic driving force and eutectic point data.

The present study reports on experimentally obtained metallic glass formation, structure and thermal stability of binary Cu–Hf alloys. It also explores whether a change in geometry of the copper cooling interface, i.e. from thick melt-spun ribbons to cylindrical rods, could improve the GFA of the binary Cu–Hf alloys, since the rate of heat transfer in cylindrical copper moulds is higher than that for thick ribbons or in wedge-shaped moulds.

Experimental procedure

Ingots with nominal compositions of $Cu_{100-x}Hf_x$ (where $25 \leq x \leq 50$ at.% and increments in $x = 5$ at.%) were prepared by arc melting mixtures of Hf (crystal bar) and Cu (sheet) having purities of 99.8 and 99.99 %, respectively. Arc melting was performed in a Ti-gettered, high purity Ar atmosphere. Each ingot was re-melted at least four times in order to obtain good chemical homogeneity. The alloy compositions represent the nominal values, though the weight losses during melting were negligible (≤0.1 %). Ribbon samples were cast at different wheel speeds by melt spinning in order to vary ribbon thickness, in a controlled atmosphere of He with an injection pressure of 0.4 bar (40 kPa) and a nozzle orifice diameter of 0.8 mm. The gap between the crucible (fused silica) nozzle and the copper wheel was approximately 5 mm. Copper die suction casting was employed to produce rods with a stepped profile, having diameters decreasing from 2–1 to 0.5 mm, each with a length of 15 mm. Phase analysis of the rods and ribbons was performed by X-ray diffraction (XRD) with a CuKα source, and samples from the transverse cross-section of the best bulk glassy alloy rods were examined by high-resolution transmission electron microscopy (HRTEM), with an accelerating voltage of 120 kV. Thermal stability was studied by differential scanning calorimetry (Perkin-Elmer DSC 7) at a heating rate of 20 K/min in Au sample pans to obtain the glass transition (T_g) and crystallisation (T_x) temperatures. The solidus (T_s) and liquidus (T_l) temperatures were determined by differential thermal analysis (DTA) at a heating rate of 20 K/min in alumina crucibles. All thermal characterisation was performed using melt-spun ribbon samples only.

Results and discussion

The analysis of glass formation for the binary alloys was carried out by melt spinning with wheel speeds varying from 5 to 35 m/s. With increasing wheel speed, the thickness of the as-spun ribbons decreased from 170 to 18 μm, as shown in Fig. 1. Consequently, there was a concurrent reduction in cooling rate with decreasing wheel speed. All the alloy ribbons exhibited high metallic lustre and those that showed a fully amorphous structure by XRD on the ribbon free surface could be easily bent through 180° without fracture. The maximum glassy length scales (x_c for melt-spun ribbons and d_c for suction cast rods) obtained by XRD for all the ribbon and bulk rod samples of the $Cu_{100-x}Hf_x$ alloy series with $x = 25$–50 at.% are summarised in Table 1. Figure 2 shows XRD patterns taken from the free surface for the binary $Cu_{100-x}Hf_x$ ($30 \leq x \leq 50$ at.%) ribbons. The $Cu_{60}Hf_{40}$ and $Cu_{65}Hf_{35}$ alloy compositions showed a fully glassy phase up to a thickness of 170 μm, corresponding to a roll speed of 5 m/s. x_c of the compositions $x = 50$, 45 and 30 sequentially decreased, showing a fully glassy phase for a ribbon thickness of 120 μm for the $Cu_{50}Hf_{50}$ and $Cu_{55}Hf_{45}$ alloys

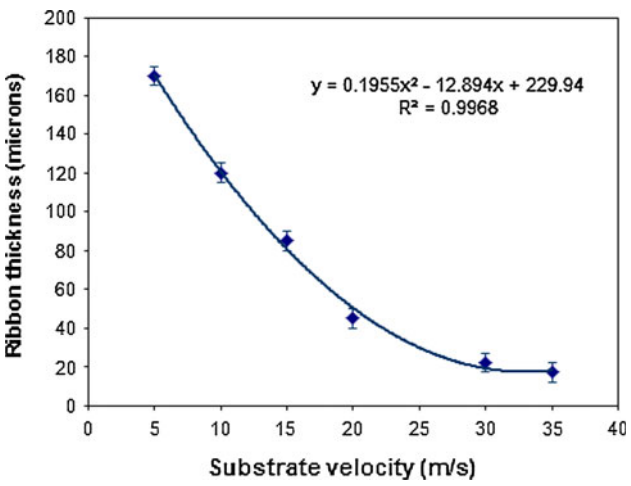

Fig. 1 Ribbon thickness as a function of wheel roll speed for the binary $Cu_{100-x}Hf_x$ ($50 \geq x \geq 30$ at.%) alloy ribbons, for a constant ejection pressure

Table 1 Critical glass-forming diameter, d_c, of rods, and of ribbons, x_c, and thermal properties for the $Cu_{100-x}Hf_x$ alloy series

Composition	d_c (mm)	T_g (K) ± 4	T_x (K) ± 4	T_m (K) ± 10	T_l (K) ± 10	T_{rg} ± 0.008	ΔT_x (K) ± 2
$Cu_{50}Hf_{50}$	0.48	757	797	1256	1423	0.53	40
$Cu_{55}Hf_{45}$	0.48	765	802	1253	1393	0.55	37
$Cu_{60}Hf_{40}$	0.6	771	810	1243	1373	0.56	39
$Cu_{65}Hf_{35}$	1	787	828	1246	1268	0.62	41
$Cu_{70}Hf_{30}$	0.18	802	817	1243	1333	0.60	15
$Cu_{75}Hf_{25}$	<0.018	728	–	1266	1398	–	–

and 45 μm for the $Cu_{70}Hf_{30}$ alloy, as shown in Fig. 2. $Cu_{75}Hf_{25}$ showed a partly crystalline structure even at the highest wheel speed. Figure 3 presents XRD patterns from the free surface for ribbons of the $Cu_{75}Hf_{25}$ alloy, cast at various roll speeds. The traces indicate that even the 18 μm thick ribbon was partly amorphous, exhibiting a crystalline peak at $2\theta = 43.64$, which corresponds to face centred cubic Cu. It was also observed that the crystalline peaks in the $Cu_{75}Hf_{25}$ alloy became progressively stronger, and the diffuse broad amorphous peak between 35 and 50 2θ became progressively weaker with increasing ribbon thickness. Phase identification shows that most crystallites in the amorphous–crystalline structure correspond to Cu, Cu_8Hf_3 and $Hf_{14}Cu_{54}$.

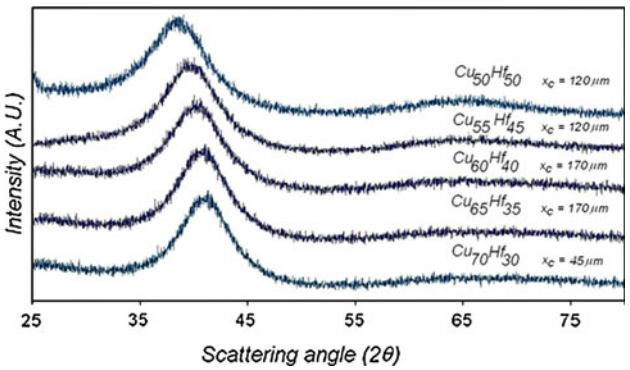

Fig. 2 XRD patterns of the critical thickness, x_c, in the binary $Cu_{100-x}Hf_x$ ($50 \geq x \geq 30$ at.%) alloy series, on the free surface of the ribbon

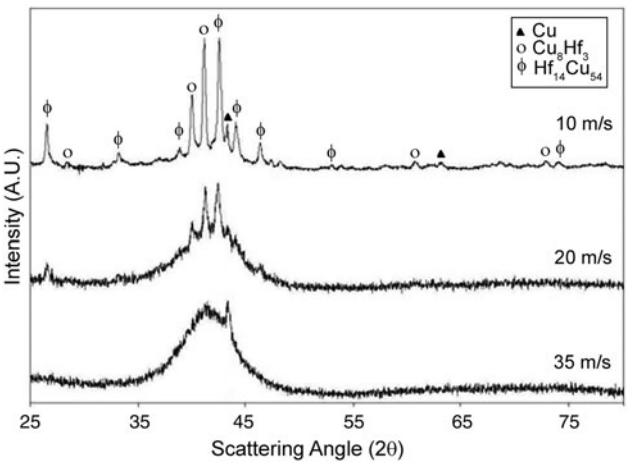

Fig. 3 XRD patterns from the free surfaces of the as-spun ribbons of $Cu_{75}Hf_{25}$ with thicknesses of 18–120 μm

According to Davies [12], the ratio between the critical glassy diameter, d_c, and the maximum thickness of a fully amorphous ribbon, x_c, is typically of the order of 4, with d_c being frequently up to 150 μm (wire) when x_c is 40 μm (ribbon). Therefore, as the binary $Cu_{60}Hf_{40}$ and $Cu_{65}Hf_{35}$ alloys have shown a glassy phase to thicknesses ≥170 μm it is thought that d_c could be ≥0.5 mm. In order to explore whether this finding is true for this study, bulk samples of $Cu_{60}Hf_{50}$, $Cu_{65}Hf_{35}$ and $Cu_{55}Hf_{45}$ alloy compositions were produced by copper die suction casting, with a stepped profile rod shape, having diameters decreasing from 2–1 to 0.5 mm, each with a total length of 15 mm. The rods produced by suction casting showed good metallic lustre and a low incidence of fabrication defects, though it was not possible to completely fill the 0.5 mm cavity; approximately 7 mm was the maximum rod length obtainable for the 0.5 mm segment. Figure 4 shows the XRD traces for the longitudinal centre-line sections of the $Cu_{55}Hf_{45}$, $Cu_{60}Hf_{50}$ and $Cu_{65}Hf_{35}$ rods produced by copper die suction casting. The XRD trace for the 0.5 mm diameter $Cu_{55}Hf_{45}$ rod sample appeared to have a broad amorphous peak with some crystalline peaks, suggesting a substantial fraction of amorphous phase. The bulk $Cu_{60}Hf_{40}$ alloy showed a critical glassy diameter, $d_c = 0.5$ mm, having an XRD pattern consisting of a broad diffraction halo between $2\theta = 30$ and 50. In contrast, the 1 mm rod diameter appeared to consist largely of crystalline peaks with a small percentage of amorphous phase. The $Cu_{65}Hf_{35}$ alloy was found to be the best glass-forming composition with a $d_c \geq 1$ mm, as the XRD trace for the 1 mm diameter as-cast rod sample showed a broad diffraction peak with no clear evidence of crystalline peaks, suggesting a fully amorphous phase. However, the XRD trace of the 2 mm diameter rod had a glassy halo with some crystalline peaks, as shown in Fig. 4. Since the stepped die diameters incremented from 1 to 2 mm, it was not possible to determine the exact d_c of this composition; therefore, it was concluded that 1 mm $\leq d_c \leq$ 2 mm.

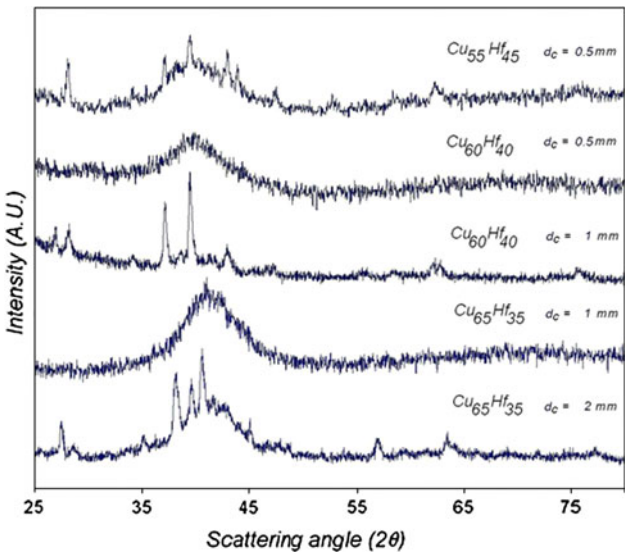

Fig. 4 XRD traces for the longitudinal centre-line sections of suction cast rods of $Cu_{55}Hf_{45}$, $Cu_{60}Hf_{50}$ and $Cu_{65}Hf_{35}$ with diameters of 0.5–2 mm

The amorphous structure of the as-cast 1 mm diameter $Cu_{65}Hf_{35}$ rod was further confirmed by HRTEM. Figure 5 shows the electron diffraction pattern and the bright-field image taken from the longitudinal centre-line section of the $Cu_{65}Hf_{35}$ rod with a thickness of 1 mm. The pattern consists of a diffuse amorphous halo, and no distinct evidence of thin crystalline rings were found anywhere across the entire specimen. In addition, no atomic ordering in the high-resolution bright-field image can be seen; these findings suggest that a single glassy phase was formed, confirming the XRD results presented in Fig. 4.

As described above, the binary $Cu_{100-x}Hf_x$ alloy series showed a glassy phase structure for ribbons in the composition range of 30–50 at.% Hf. The 25 at.% Hf alloy had a coexisting crystalline and amorphous structure, as revealed by XRD. According to the Cu–Hf equilibrium phase diagram [13], the crystalline phases in the $Cu_{75}Hf_{25}$ alloy are probably Cu_3Hf_2 and Cu_5Hf_2 [13]. However, the first crystallisation peak observed in this alloy was attributed to an excess of Cu phase, as shown in Fig. 3. Table 1 shows the critical glassy diameter, d_c, estimated by conversion from ribbon data for alloys with $d_c < 0.5$ mm. The conversion factor from the critical thickness for fully glassy ribbon, x_c, is estimated to be of the order of 4 [12]. This assumes that the interfacial heat transfer coefficients are similar for the melt spinning and rod casting processes, and that Newtonian cooling is the operative heat transfer mechanism. This criterion proved to be approximately true for water bath wire casting versus chill block melt spinning [12] and it seems that for rod casting versus chill block melt spinning also it is approximately true. More experimental evidence based on different alloy systems is required in order to validate the applicability of this criterion.

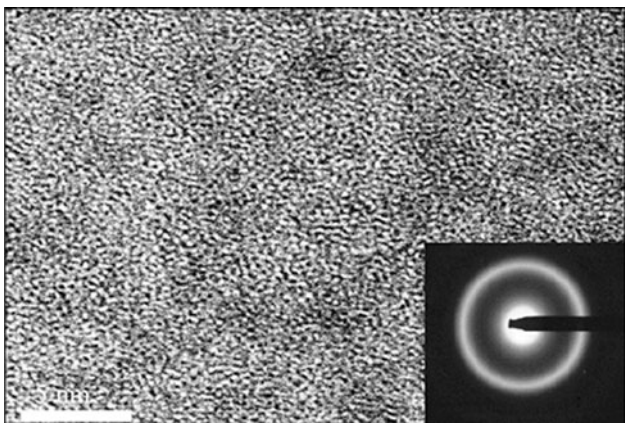

Fig. 5 HRTEM bright-field image and electron diffraction pattern for the longitudinal centre-line section of the as-cast 1 mm diameter rod of $Cu_{65}Hf_{35}$

Figure 6 shows DSC curves for the melt-spun ribbons of this alloy series at a heating rate of 20 K/min, where T_g and T_x are marked with arrows. The values of T_g, T_x, T_m and T_l are also presented in Table 1. Although no clear glass transition is observed for 30 at.% Hf, the alloys containing 35–50 at.% Hf exhibit distinct glass transitions, followed by the supercooled liquid region and crystallisation. However, for the alloy containing 25 at.% Hf, which was partially crystalline, a significantly lower transition temperature of 725 K was observed (since T_g and T_x are not clear they were taken at the same point), followed by a large slope/peak, which could be related to the growth of

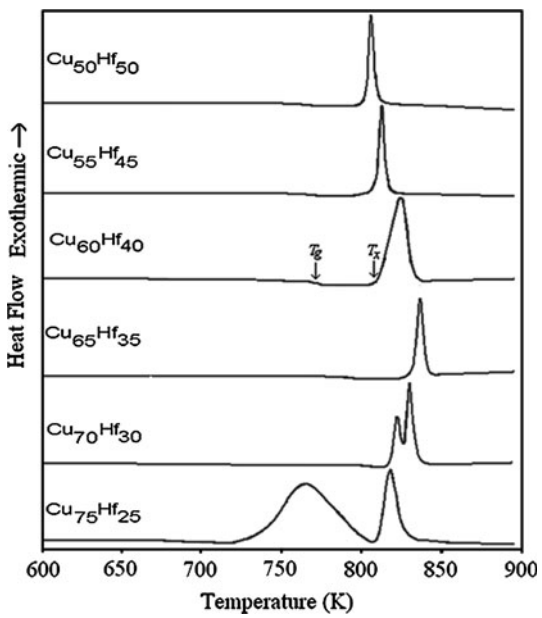

Fig. 6 DSC curves of the melt-spun $Cu_{100-x}Hf_x$ glassy alloys, at a heating rate of 20 K/min

the crystalline phase detected by XRD. The values of T_g and T_x increased with increasing Cu content from 50 to 65 at.%, despite the fact that the Hf has a much higher cohesive energy than Cu, i.e. −422 and −1314 kJ/mol, respectively [14].

It is also observed that the supercooled liquid region defined by the temperature interval between T_g and T_x (ΔT_x ($=T_x - \Delta T_g$)) showed a relatively constant value of approximately 38 ± 3 K over the range 50–65 at.% Cu, but appears to narrow considerably for 70 at.% Cu. ΔT_x then diminishes for 75 at.% Cu, since this composition did not show detectable evidence of the glass transition event, probably due to its partly crystalline structure (Fig. 7). With the substitution of Hf for Cu over the range 35–50 at.% Hf, T_l decreased, having a minimum of 1263 K at 35 at.% Hf or 65 at.% Cu, in good agreement with the Cu–Hf equilibrium diagram [13]. At lower Hf contents of 30 and 25 at.%, T_l increased progressively up to 1398 K.

The values of the reduced glass temperature, T_{rg} ($T_{rg} = T_g/T_l$), are plotted as a function of Cu content in Fig. 7 The magnitude of T_{rg} increases with increasing Cu content from 0.53 to 0.62 for $Cu_{50}Hf_{50}$ and $Cu_{65}Hf_{35}$, respectively, and then decreases to its lowest value of 0.52 for the $Cu_{75}Hf_{25}$ alloy. The maximum obtainable d_c thus corresponds to a maximum in T_{rg}. Since T_s is approximately constant for all alloys investigated, it is the low T_l that appears to be determining the good glass formation observed here.

As the alloys $Cu_{65}Hf_{35}$ and $Cu_{70}Hf_{30}$ had values of $T_{rg} > 0.60$ it might be expected that 2 mm diameter fully glassy rods could be castable within this composition range. However, attempts to produce rods larger than 2 mm diameter were not successful, as the XRD patterns in Fig. 4 showed crystalline peaks. These results clearly show that $Cu_{65}Hf_{35}$ is the best glass former in this series of binary alloys, having a d_c of at least 1 mm. Duan et al. [3] reported that the alloy $Cu_{66}Hf_{34}$ could be readily cast into 2 mm thick fully amorphous ribbons. This alloy falls into the values where T_l is markedly reduced, between 60 and 70 at.% Cu, as shown in Table 1. These results suggest that in binary systems the strong composition dependence of the liquidus temperature may account for the relatively narrow composition range of high glass formability and may explain why the other compositions studied were not successful in producing BMGs [15].

$Cu_{65}Hf_{35}$ is located near the $Cu_{61.4}Hf_{38.6}$ eutectic composition in the Cu–Hf system, which has the lowest T_l. This is consistent with the relatively high GFA (when considering d_c) of the $Cu_{65}Hf_{35}$ alloy, since deep eutectics are known to exhibit a suppressed T_l, and concurrent good glass formation. The size of T_{rg} for this alloy was the greatest among the alloys investigated in this series, as shown in Fig. 7. Notwithstanding the limitations of the parameter T_{rg}, or any other parameter based on transition temperatures for predicting GFA, due to the medium–high critical cooling rates for glass formation required in the Cu–Hf system and the relatively narrow range of alloy compositions investigated, there was satisfactory correlation between T_{rg} and the experimentally observed d_c. The extent of the undercooled liquid region ($\Delta T_x = T_x - T_g$) is another parameter that is commonly used for predicting GFA [16–19]. Although some BMGs are characterised by large values of ΔT_x (e.g. Zr-based BMGs), there does not appear to be a clear correlation in the present case between the experimental GFA, measured by d_c, and ΔT_x. The plot of ΔT_x, as a function of alloy composition presented in Fig. 7, shows constant values between the $Cu_{50}Hf_{50}$ and $Cu_{65}Hf_{35}$ alloys, and so does not account for the large variation in GFA observed across the alloy range studied.

From theoretical studies, Basu et al. [9] studied the metallic glass formation range in the Cu–Hf system. As already mentioned, they found that the GFA for this system lies between 10 and 80 at.% Hf (Fig. 8). This agrees well with the experimental results reported in this work and for metallic glasses with at least one dimension below 150 microns (ribbons, wires and powders). However, although this approach works well for conventional metallic glasses, and gives a plausible explanation for metallic glass formation in the Cu–Hf system, the BMG formation range cannot be entirely explained by this model. From Fig. 8, it

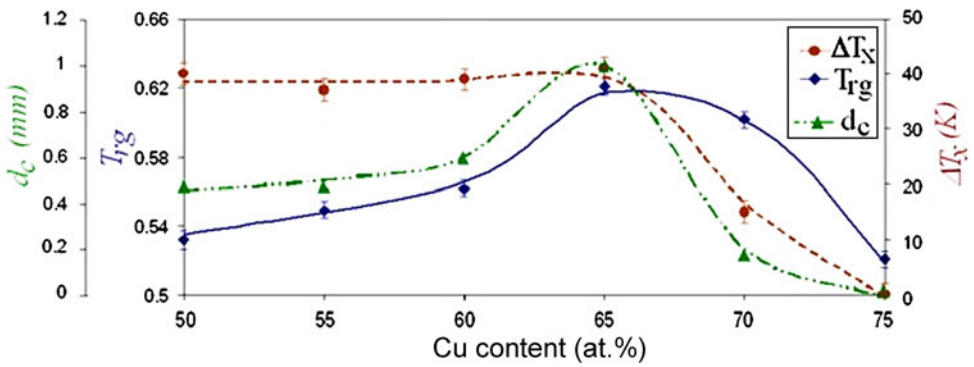

Fig. 7 Plots of d_c, T_{rg} and ΔT_x for binary $Cu_{100-x}Hf_x$ alloys

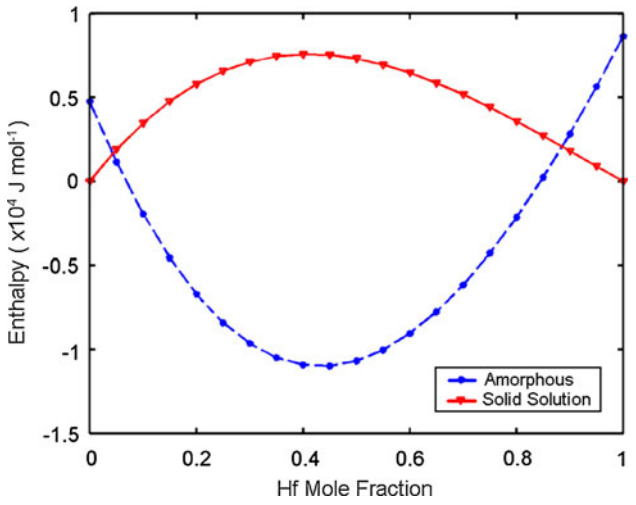

Fig. 8 Plot of the enthalpy versus composition for the binary Cu–Hf alloy system. Modified from Ref. [9]

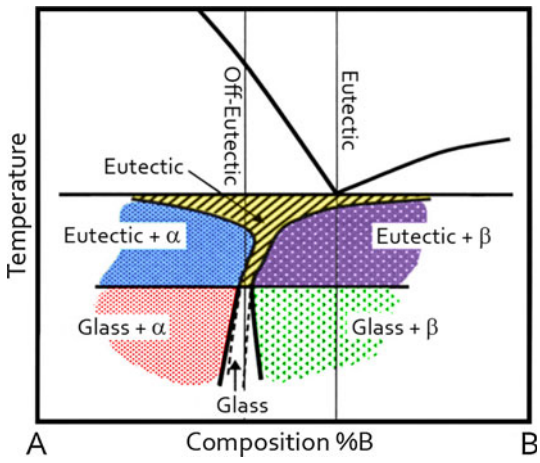

Fig. 9 Schematic diagram of a binary system showing the glass formation range in an off-eutectic composition. (Modified from Ref. [21])

might be thought that the optimum glass-forming compositions could be found at the local minima of the enthalpy vs composition diagram for the binary Cu–Hf system, but none of the BMG compositions reported here or in the literature lie near such minima.

It is difficult to theoretically predict the exact composition for BMG formation in binary alloys. This is in part due to d_c being commonly located at just one point, or a very narrow composition range, on the binary phase diagram; it has been observed that even a small change in composition can drastically alter GFA [20–22]. In binary systems, the eutectic point has historically been associated with the greatest GFA. However, as in our case and in several reported binary BMGs and for $Cu_{65}Hf_{35}$ in the instance of this study, it has been found at off-eutectic compositions. According to Ma and coworkers [21] in off-eutectic compositions the glassy phase will be competing with many other phases, including, and in particular, the eutectic composition. This was attributed to the fact that the kinetic constraints during the casting process can be the factor controlling crystallisation at compositions away from the eutectic point. As a result, the corresponding composition zone could be asymmetric and even exclusive of the eutectic composition, as shown in Fig. 9 [21]. Based on this, they concluded that GFA of a eutectic alloy or near eutectic system depends on the type of eutectic, i.e. symmetric or asymmetric-coupled zones. For the alloy systems with symmetric eutectic-coupled zones, the best composition should be at, or very close to, the eutectic composition. For the alloys with asymmetric eutectic-coupled zones, however, the best composition should be off-eutectic, probably towards the side of the faceted phase with high entropy in the phase diagram. In this area, the microstructure of the alloy in a cast sample cooled to below T_g would change from a primary phase in an amorphous matrix, then to another primary phase in the amorphous matrix and finally forming a fully amorphous phase (Fig. 9). Based on the above, it could be speculated that the bulk $Cu_{65}Hf_{35}$ glassy composition is located at an asymmetric-coupled zone on its corresponding eutectic.

Topological studies [23, 24] have shown that certain atomic-size mismatch and efficient atomic packing may enhance GFA of a system. Using the model proposed in Ref. [23] we can calculate the preferred values, R^*, for the ratio (R) of the solute atom radius (r_x) to the solvent atom radius (r_y) ($R = r_x/r_y$). In the present system, the atomic radii of the component atoms are: Cu = 0.127 nm and Hf = 0.1577 nm, respectively [23]. Thus, $R_{Hf/Cu} = 1.242$. Comparing this value with the critical values listed in Table 1 of Ref. [23], good agreement can be found between $R_{Hf/Cu}$ and R^*17 (=1.248). Therefore, the model could predict the $Cu_{90}Hf_{10}$ and $Hf_{82}Cu_{18}$ compositions, with atomic packing efficiency of 43.89 and 43.25 %, respectively. It is noteworthy that from this result, the GFA for the Cu–Hf system lies between 10 and 82 at.% Hf, being rather similar to that reported by Basu et al. [9] where, as mentioned above, the range for metallic glass formation lies between 10 and 80 at.% Hf.

Conclusions

The GFA of the binary alloy series $Cu_{100-x}Hf_x$ (x = 50, 45, 40, 35, 30, 25 at.%) has been investigated and discussed. Glass formation was observed in ribbons of various thickness for x = 30–50 at.%, and the critical casting thickness, x_c, was found to be the greatest when x = 35 and 40 at.%. A criterion for converting from x_c for ribbons to critical diameter, d_c, in cast rods proposed by Davies [12],

was applied and showed good correlation. $Cu_{65}Hf_{35}$ exhibited a large critical diameter of 1 mm, and can thus be considered a BMG. The high GFA exhibited by this system is considered within the context of thermal parameters ΔT_x and T_{rg}. The magnitude of ΔT_x was approximately constant for all compositions studied, and so could not justify the observed results; however, T_{rg} was found to be the greatest in $Cu_{65}Hf_{35}$. By comparing T_l it is found that it is the lowest for $Cu_{65}Hf_{35}$, which is also close to the eutectic point where glass formation would be considered to be the greatest. The results of the Miedema [9, 10] and the efficient solute centred cluster packing [24] models show remarkable similarities; Miedema's model predicts the range for metallic glass formation to be between 10 and 82 at.% Hf, and the efficient packing model predicted a range within 10–80 at.% Hf. Finally, the $Cu_{65}Hf_{35}$ composition which showed the highest GFA could be additionally explained by it being just off-eutectic at an asymmetric-coupled zone.

Acknowledgements This work was supported by PAPIIT-UNAM through Grant No. IB100712. A. Tejeda Cruz, J. J. Camacho, G. Aramburo, E. A. Caballero, R. Reyes, E. Contreras, C. Flores, E. Sánchez, J. Morales-Rosales and C. Gonzalez are also acknowledged for the technical support.

References

1. Guo FQ, Poon SJ, Shiflet GJ (2004) Appl Phys Lett 84:37
2. Tang MB, Zcxhao DQ, Pan MX, Wang WH (2004) Chin Phys Lett 21:901
3. Duan G, Xu D, and Johnson W. L, (2005) High Copper Content Bulk Glass Formation in Bimetallic Cu–Hf System, Metall. and Mater. Trans. A, 36a, 455
4. Inoue A, Zhang W (2004) Mater Trans, JIM 45:584
5. Xia L, Ding D, Shan ST, Dong YD (2006) J Phys: Condens Matter 18:3543
6. Jia P, Xu J (2009) J Mater Res 24–1:96
7. Angell CA (1995) Science 267–5206:1924
8. Busch R, Masuhr A, Johnson WL (2001) Mater Sci Eng, A 304–306:97
9. Basu J, Murty BS, Ranganathan S (2008) J Alloy Compd 465:163
10. Miedema AR (1976) Philips Tech. Rev. 36:217
11. Li C, Chen SC, Du Z, Wang N (2011) Intermetallics 19:1678
12. Davies HA (1994) In: Proceedings of the 4th international workshop on nonocrystalline solids: metallic glass formation revisited from nanostructured and nonocrystalline materials, World Scientific Press, Spain, p 3
13. Massalski TB (1990) Binary alloy phase diagrams. ASM International, Materials Park
14. Turchanin MA, Agraval PG (2008) Powder Metall Met Ceram 47:26
15. Shi LL, Xu J, Ma E (2008) Acta Mater 56–14:3613
16. Figueroa IA, Rawal R, Stewart P, Carroll PA, Davies HA, Todd I, Jones H (2007) J Non-Cryst Solids 353:839
17. Figueroa IA, Davies HA, Todd I, Yamada K (2007) Adv Eng Mater 9:496
18. Figueroa IA, Davies HA, Todd I, Verduzco JA, Hawksworth P (2006) Adv Technol Mater Mater Process J (ATM) 8:146
19. Figueroa IA, Zhao H, González S, Davies HA, Todd I (2008) J Non-Cryst Solids 354:5181
20. Ma D, Tan H, Wang D, Li Y, Ma E (2005) Appl Phys Lett 86:191906
21. Wang D, Lia Y, Sun BB, Sui ML, Lu K, Ma E (2004) Appl Phys Lett 84:4029
22. Figueroa IA, Davies HA, Todd I (2009) Phil Mag 89–27:2355
23. Miracle DB (2006) Acta Mater 54:4317
24. Miracle DB (2004) Nat Mater 3:697